*Iraqi Journal of Physics, 2023* *Vol. 21, No.3, PP. 92-101*
*https://doi.org/10.30723/ijp.v21i3.1126* *P-ISSN: 2070-4003*
*E-ISSN: 2664-5548*

# Fabrication and Characterization of Silicon Nanowires Heterojunction Solar Cell

**Hana. H. Inaya[1a*] and Mazin A. Mahdi[1b]**
[1]*Department of Physics, College of Science, University of Basrah, Basrah, Iraq*
[b]E-mail: m.a.mahdi@uobasrah.edu.iq
[a*]Corresponding author: hanainaya0@gmail.com

## Abstract

Silicon nanowire arrays (SiNWs) are created utilizing the metal-assisted chemical etching method with an Ag metal as a catalyst and different etching time of 15, 30, and 60 minutes using n-Si (100). Physical properties such as structural, surface morphology, and optical properties of the prepared SiNWs are studied. The diameter of prepared SiNWs ranged from 20 to 280 nm, and the reflectance in the visible part of the wavelength spectrum was less than 1% for all prepared samples. The obtained energy gap of prepared SiNWs was around 2 eV, which is higher than the energy gap of bulk silicon. X-ray diffraction (XRD) has diffraction peaks at 68.70° for all prepared samples. The heterojunction solar cell was fabricated based on the n-SiNWs/ P3HT/PEDOT: PSS structure. The heterojunction solar cell produced for 60 minutes has the highest $J_{sc}$ of 11.55 mA.cm$^{-2}$ and a conversion efficiency of 0.93%. Based on SiNWs prepared for etching time of 15 min, the solar cell demonstrated $J_{sc}$ and $V_{oc}$ of 2.73 mA/cm$^2$ and 0.46 V, respectively, and a conversion efficiency of 0.34%.

**Article Info.**

**Keywords:**
*Conjugated polymer, P3HT, SiNWs, Electroless chemical etching, Conversion efficiency.*

**Article history:**
*Received: Apr. 26,2023*
*Revised: Aug. 12, 2023*
*Accepted: Aug.14, 2023*
*Published: Sep. 01,2023*

## 1. Introduction

One-dimensional (1-D) semiconductors such as nanowires, nanorods, and nanoribbons have several unique advantages, including high crystallinity, self-assembly, a high surface-to-volume ratio, quantum confinement effects, as well as slow electron–hole recombination [1, 2]. Silicon-based nanowires (SiNWs) are particularly attractive because of silicon's focal role in the semiconductor industry. SiNW arrays have distinct physical and optical properties, allowing them to be used as basic components for a variety of applications, such as solar cells [3-6], thermoelectric systems [7-9], Li-ion batteries [10], field-effect transistors (FETs) [11-13], bio and chemical sensors [14, 15], photodetectors [16-18] and photocatalysts [19, 20]. SiNWs are distinct and sensitive to surface analyte adsorption because of their high surface area-to-volume ratio and repeatable electronic properties. Silicon-based materials with enhanced optical properties can increase the efficiency of photovoltaic solar cells. SiNW arrays are used to produce large areas of SiNW solar cells [21]. Light absorption increased with these nanowire arrays compared with planer silicon solar cells [22-24]. Furthermore, studies on nanostructures embedded in polymer matrices show that they are widely used in the fabrication of hybrid solar cells (HSCs) [25, 26]. Semiconducting polymers and inorganic nanomaterials have good photoconductive capabilities because inorganic semiconductors can separate photogenerated excitons effectively and have high electron mobility. Poly(3-hexylthiophene) (P3HT) could become a more acceptable matrix for hybrid nanocomposite-based electronics. This is because it has higher hole mobility and a lower band gap than other polymeric semiconductors [27]. In addition, poly (3,4-ethylene dioxythiophene) (PEDOT): polystyrene sulfonate (PSS) has been widely used in the production of hybrid solar cells (HSCs) because of its high conductivity, transparency, and wide band gap. The present work aims to fabricate heterojunction solar cells based on silicon nanowire arrays prepared with different etching times.

## 2. Experimental Work

### 2.1. SiNW Array Preparation

Si (100) wafer with a thickness of (370 ± 25) μm was double-side polished, and a resistivity of 0.1−0.5 Ω.cm was cut into 0.7 cm × 0.7 cm using metal-assisted chemical etching (MACE) [28]. First, the Si wafer was cleaned with piranha solution ($H_2SO_4/H_2O_2$) (3:1) at 90 °C for 20 minutes to remove the surface of organic residues. After that, the wafers were submerged in diluted hydrofluoric (HF) acid at 10% for 5 minutes to remove the $SiO_2$ native oxide from the wafer surface. The cleaned wafer was then immersed for 60 seconds in an aqueous solution of 5 M HF and 0.02 M $AgNO_3$ to deposit Ag particles. The samples were then immediately transferred to an etching solution containing HF 5M and 0.2M $H_2O_2$ for various periods of time (15, 30, and 60 minutes) to produce the vertically aligned SiNWs, followed by a 10 second dip in nitric acid to remove the Ag nanoparticles.

### 2.2. Solar Cells Fabrication

At first, fluorine-doped tin oxide glass (FTO) was sonicated in acetone and ethanol to clean the substrates, which were then washed with deionized water. A layer of PEDOT:PSS (Clevis PH1000), which was diluted with 20 wt% isopropanol and 5 wt% dimethylsulfoxide (DMSO) to increase the conductivity of the pure PEDOT:PSS film and thus improve the power conversion efficiency, was spin-coated on the FTO substrate for 30 seconds at a speed of 2000 rpm. Aluminum (Al) was deposited onto the back side of the Si wafer by thermal evaporation before polymer coating to establish an ohmic contact. P3HT was spin-coated onto SiNWs for 30 seconds at 4000 rpm. Owing to the capillary effect, blended PEDOT:PSS easily filled SiNW gaps to form a core–sheath heterojunction. The PEDOT:PSS/FTO/glass substrate was then bonded with a clip to the SiNWs/P3HT to finish the hybrid solar cell manufacturing [29, 30]. Finally, the devices were roasted for 10 minutes at 120 °C in an air vacuum oven to remove the solvent. Fig. 1 depicts the typical hybrid solar cell device structure used in the current study. This device can be regarded as a tandem double-junction solar cell [31, 32]. The HOMO of the P3HT was positioned to inject holes into PEDOT:PSS, and therefore into the FTO electrode. Fig. 1 depicts the typical hybrid cell device structure used in the current study. The HOMO of P3HT was positioned to inject holes into PEDOT:PSS and, consequently, into the FTO electrode. The LUMO of P3HT was positioned well above the Fermi level of n-SiNWs, implying that electron collection should be efficient at the silicon interface. The SiNW electrons would be collected at the aluminum electrode [33]. Fig. 1 (a) depicts the device fabrication. Energy levels relative to the vacuum level and corresponding to the components of the photovoltaic cells are shown in Fig. 1(b).

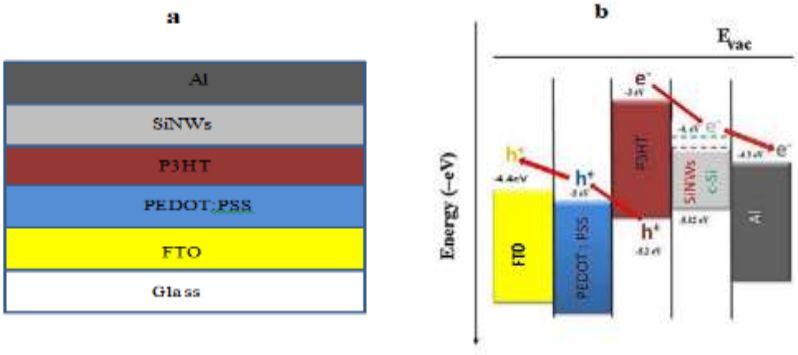


***Figure 1: (a) Schematic representation of the Al/n-SiNWs/P3HT/PEDOT: PSS/FTO HSCs. (b) Schematic energy level diagram and possible charge transportation of HSCs.***

## 3. Results and Discussion

### 3.1. Optical Properties

The reflectance measurements were obtained at a range of 300-1000 nm, which corresponds to the principal spectrum irradiance of sunlight at air mass (AM) 1.5 and is beneficial for Si solar cells [34]. Fig. 2(a, b) depicts the reflectance spectra of a Si wafer and SiNWs prepared with varied etching periods. The reflectivity of Si wafers is quite high, exceeding 88% and 65% in the ultraviolet (UV) regions and decreasing in the visible region to 48%, as shown in Fig. 2a. While SiNWs show low reflectance over the entire spectral range, this decrease in reflectance could be related to light harvesting and light scattering interactions between densely packed SiNWs [35-37]. This remarkable property suggests that SiNW arrays are a good candidate for antireflective surfaces and absorption materials in photovoltaic cells [38]. Fig. 2b shows the reflectance of the SiNWs about 0.26%, 0.22%, and 0.14% at a wavelength of 820 nm, for different etching times of 15, 30, and 60 min, respectively. In other words, the reflectance decreases gradually with increased etching time [39].

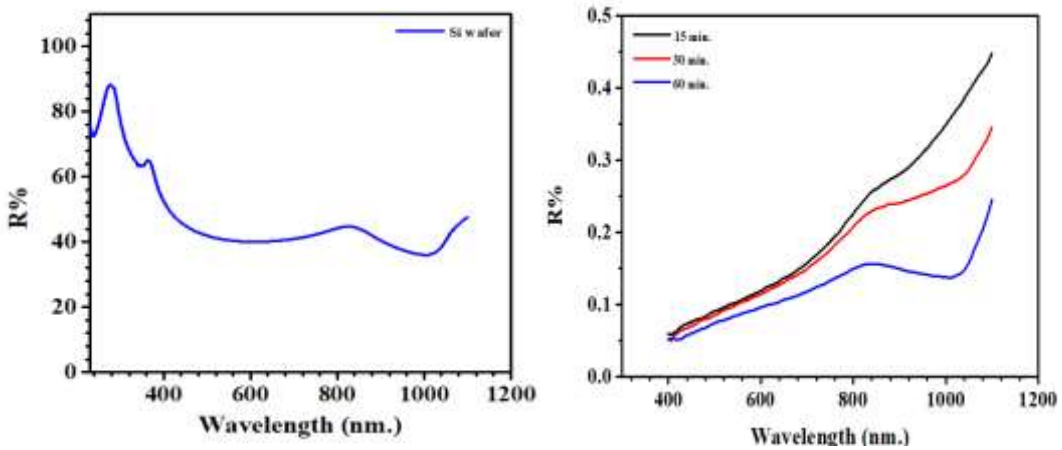


***Figure 2: (a) and (b) reflectance spectra of Si and SiNWs at etching times of 15, 30, and 60 min***

The energy gap of Si and SiNW films was calculated using the Tauc relation from the reflectance spectra for different etching times. Because of light absorption by the substance, the reflectivity dropped from its highest value, $R_{max}$ to its minimum value, $R_{min}$. To determine the band gap of a semiconductor, a line graph was made between $[\ln (R_{max}-R_{min}) / (R-R_{min})]^2$ and the energy gap [40, 41]. Fig. 3 represents the energy gap for the Si wafer and SiNWs prepared with varied etching times of silicon. The energy gap of the Si wafer is 1.12 eV, as shown in Fig. 3a; it gradually increases to 1.54, 1.6, and 1.7 eV for the SiNWs as etching times are increased to 15, 30, and 60 min, respectively, as shown in Fig. 3b-d.

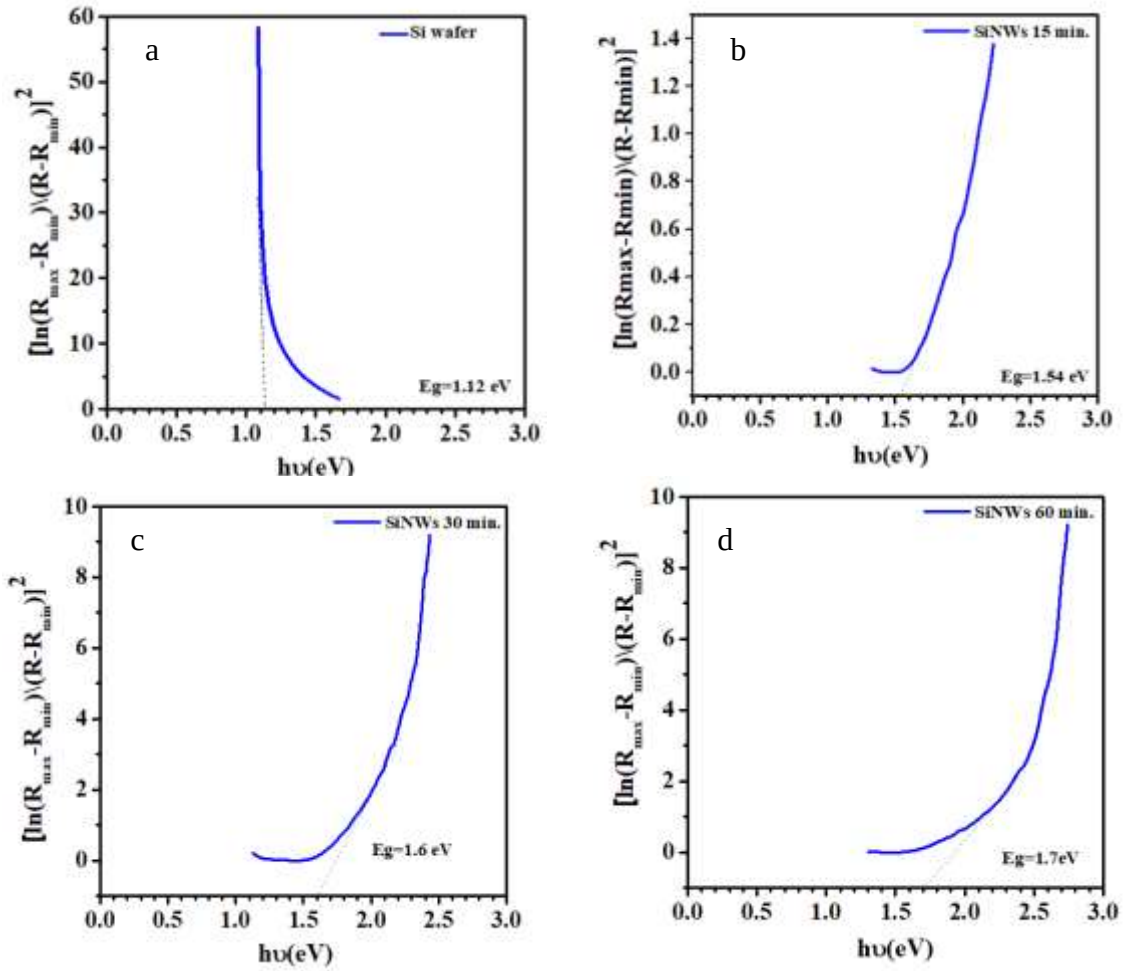


***Figure 3: Variation of [ ln ($R_{max}$-$R_{min}$)/(R-$R_{min}$)]$^2$ with hυ for the Si and prepared SiNWs at different etching times (15, 30, and 60 minutes).***

### 3.2. XRD Analysis

The X-ray diffraction (XRD) method was utilized to investigate the crystal structure of samples prepared for silicon. Fig. 4 depicts the XRD spectra of the Si wafer and SiNWs prepared at various etching times. All of the samples show a peak at 68.7° conformable to the lattice planes of (400) [42], indicating the high crystallinity of nanowires [43]. There are no further XRD peaks in the XRD patterns, indicating that no $SiO_2$ layer has formed on the surface of the prepared SiNWs. After MACE processing, the majority of the Si crystal structure is preserved on SiNWs, meaning that the SiNWs retain the unique photoelectrochemical characteristics of Si [44].

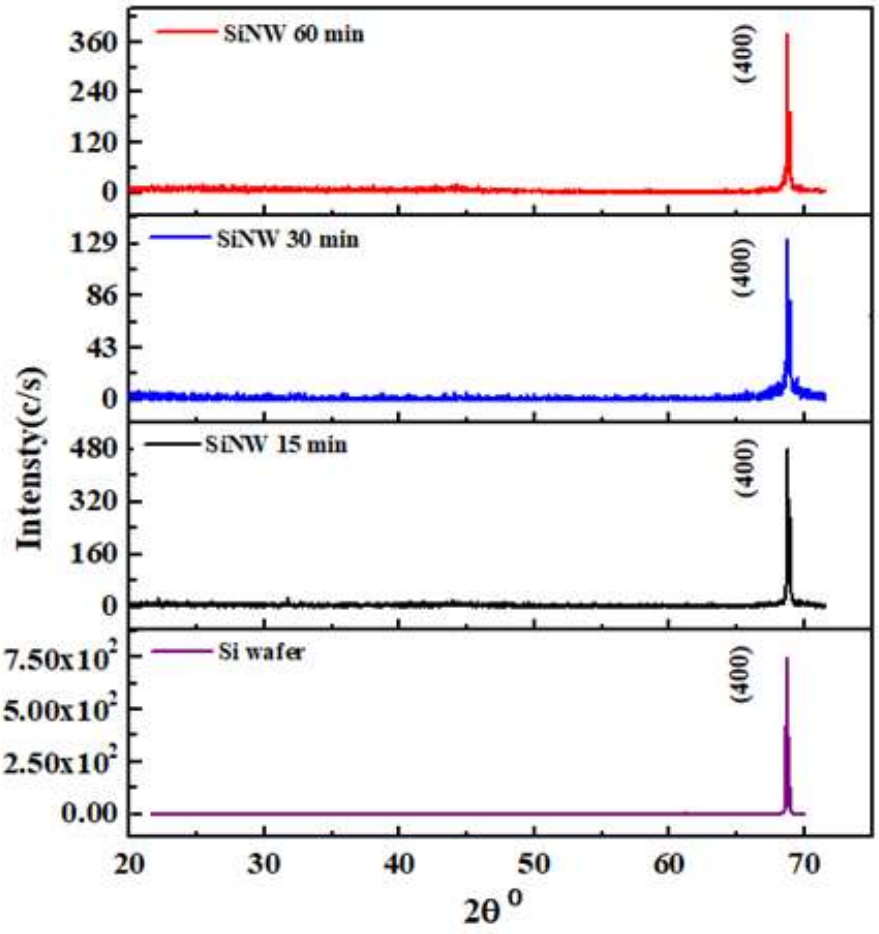


***Figure 4: XRD pattern of the Si wafer and SiNWs at different etching times.***

### 3.3. Surface Morphology

Fig. 5(a-f) shows the FE-SEM images of the SiNWs prepared for different etching times with diameter distribution. Image J software was used to measure the diameters of all prepared SiNWs. The diameters of the SiNWs prepared with an etching time of 15 minutes in the range of 20–280 nm decrease to the range of 20–200 nm for SiNWs prepared with an etching time of 30 minutes, whereas those using an etching time of 60 minutes decrease to the range of 20–220 nm. Observe that the etching is causing the formation of nanowires with clustered tips that form the beams. It is assumed that the van der Waals attraction is responsible for the formation of these beams [45]. When the etching time increases, the number density of nanowires increases noticeably due to the enhanced flexibility of the SiNWs when the etching time is extended. Earlier investigations undertaken by other researchers revealed similar findings [46, 47].

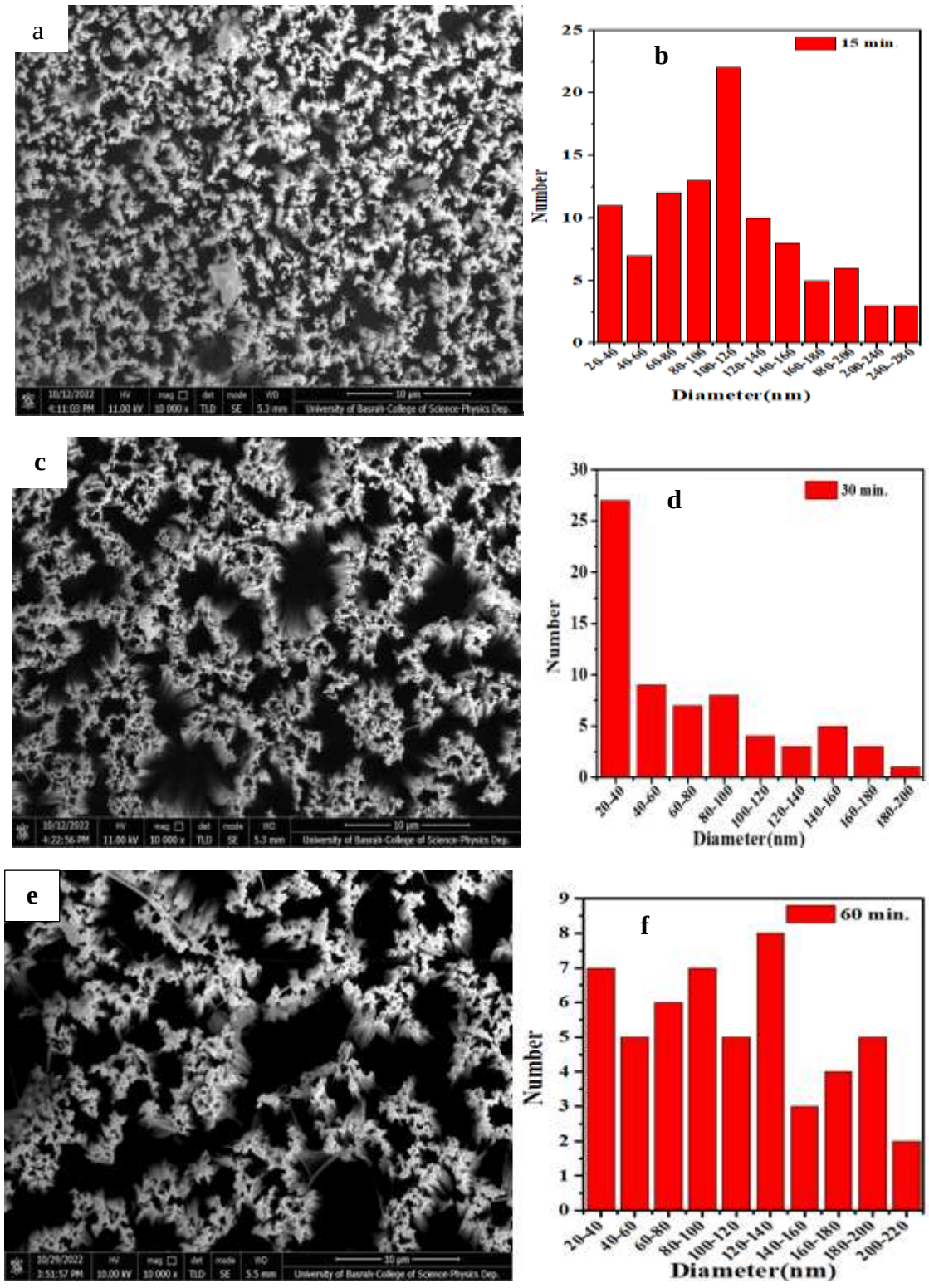


***Figure 5: Fig. 4.5(a–f): FESEM images with diameters distribution of the SiNWs at various etching times (15, 30, and 60 min).***

## 4. J-V Characterization of HSCs

In Fig. 6, the J-V characterization of the Al/SiNWs/P3HT/PEDOT:PSS/FTO heterojunction device is depicted with various etching times of SiNWs (15, 30, and 60 minutes), respectively. The solar cell that was prepared at an etching time of 15 minutes has the lowest efficiency of the solar cell η of 0.34%, while the highest η that the solar cell prepared for 60 minutes is 0.93%. As a result, the increased etching time led to increased conversion efficiency. SiNWs at etching for 60 minutes have provided a perfect environment for photon conversion to an electron. This could be due to increasing absorption for increased etching time and low reflectance, which led to high separation efficiency of the pair hole –electron. Chen et al. and Khanyile et al. also observed similar effects [48, 49]. Table 1 shows the properties and parameters of the solar cell at different etching times, where S1, S2, and S3 represent the Al/SiNWs/P3HT/PEDOT:PSS/FTO heterojunction solar cells prepared at various etching times (15, 30, and 60 min), respectively.

The J-V characteristic of the prepared solar cell was investigated under illumination by a solar simulator. Where can be calculated all the solar cell parameters, such as fill factor (FF), open circuit voltage ($V_{oc}$), short circuit current ($I_{sc}$), efficiency solar cell (η), series resistance ($R_s$), and shunt resistance ($R_{sh}$). The J-V curve is a straight line with a slope determined by $1/R_{sh}$ at negative and low voltages and a second straight line with a slope regulated by $1/R_s$ at high positive voltages ($1/R_s$ = dJ/dV) [50]. Table 1 depicts solar cell parameters**.** The greatest device performance was achieved for the SiNWs that were prepared for an etching time of 60 min with η of 0.93%, FF of 24%, $J_{sc}$ of 11.55 mA.cm$^{-2}$ and, $V_{oc}$= 0.335V.

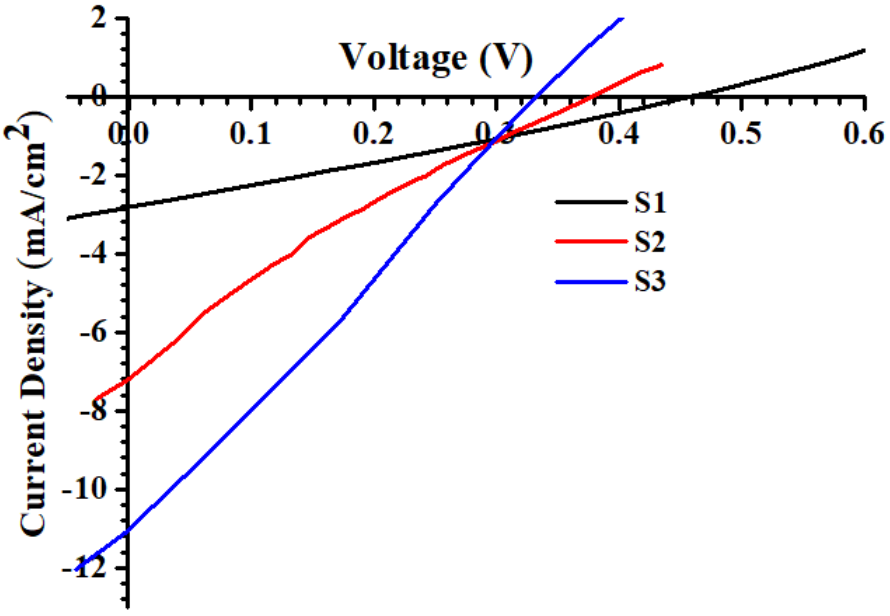


***Figure 6: J-V properties of the Al/SiNWs/P3HT/ PEDOT: PSS /FTO heterojunction device prepared at various etching times of SiNWs (S1=15 min,S2=30min and S3=60min), respectively.***

***Table 1: The characteristics of I-V Al/ SiNWs/P3HT/PEDOT: PSS/FTO with different etching times for SiNWs.***

| Device | Etching time of SiNWs(min) | $V_{oc}$ (V) | $J_{sc}$ (mA/cm$^2$) | FF (%) | $R_{Seires}$ (Ω) | $R_{Shunt}$ (Ω) | η (%) |
|---|---|---|---|---|---|---|---|
| S1 | 15 | 0.46 | 2.73 | 21 | 112.22 | 108.035 | 0.34 |
| S2 | 30 | 0.382 | 7.359 | 20 | 152.54 | 61.287 | 0.56 |
| S3 | 60 | 0.335 | 11.55 | 24 | 69.578 | 57.578 | 0.93 |

## 5. Conclusions

In summary, SiNWs' heterojunction devices have been fabricated. The SiNWs are synthesized using a MACE technique with varying etching times. All of the formed SiNWs have a very low optical reflectance (0.3%) in the 300-1000 nm wavelength region, which decreases gradually with increasing an etching time. The heterojunction devices based on SiNWs that were constructed for etching time of 15 minutes had the lowest value of η of 0.34%, and $J_{sc}$ of 2.73 mA/cm$^2$. While the heterojunction devices based on SiNWs that were prepared for etching time of 60 minutes exhibited the highest value of η that of 0.93% and $J_{sc}$ of 11.55 mA/cm$^2$. In conclusion, the increase in etching time led to an increase in conversion efficiency.

## Conflict of interest

The authors declare that they have no conflict of interest.

## References

1. M. Mahdi, J. Hassan, S. Ng, Z. Hassan, and N. M. Ahmed, Phys. E: Low-dimen. Sys. Nanostruct. **44**, 1716 (2012).
2. M. Mahdi, J. Hassan, S. Ng, and Z. Hassan, J. Crys. Grow. **359**, 43 (2012).
3. H. Al-Taay, M. Mahdi, D. Parlevliet, and P. Jennings, Silicon **9**, 17 (2017).
4. V. Kashyap, C. Kumar, V. Kumar, N. Chaudhary, and K. Saxena, Phys. B: Conden. Mat. **638**, 413953 (2022).
5. H. Li, S. Yang, J. Hu, Z. Zhang, P. Tang, Y. Jiang, L. Tang, and B. Zou, Mat. Sci. Semicond. Proces. **146**, 106661 (2022).
6. S. M. Mishra, S. Dey, T. Singha, S. Mandal, A. K. Dehury, Y. S. Chaudhary, and B. Satpati, Mat. Res. Bull. **164**, 112262 (2023).
7. A. Uesugi, S. Nishiyori, K. Sugano, and Y. Isono, in 36$^{th}$ International Conference on Micro Electro Mechanical Systems (MEMS), IEEE, 2023, p. 701.
8. G. W. Jeon, S.-H. Lee, J.-S. Jo, W. Huang, T. Fujigaya, and J.-W. Jang, Mat. Today Ener. **29**, 101109 (2022).
9. S. Mousavi, S. Davatolhagh, and M. Moradi, Phys. E: Low-dimen. Sys. Nanostruc. **118**, 113889 (2020).
10. G. Sandu, M. Coulombier, V. Kumar, H. G. Kassa, I. Avram, R. Ye, A. Stopin, D. Bonifazi, J.-F. Gohy, and P. Leclère, Sci. Rep. **8**, 9794 (2018).
11. X. Song, T. Zhang, L. Wu, R. Hu, W. Qian, Z. Liu, J. Wang, Y. Shi, J. Xu, and K. Chen, Advan. Sci. **9**, 2105623 (2022).
12. A. Lale, A. Grappin, A. Lecestre, L. Mazenq, J. Launay, and P. Temple-Boyer, Thin Sol. Fil. **764**, 139609 (2023).
13. P. Kumar and B. Raj, Microelect. J. **137**, 105826 (2023).
14. K.-I. Chen, B.-R. Li, and Y.-T. Chen, Nano Today **6**, 131 (2011).
15. Y. Cui, Q. Wei, H. Park, and C. M. Lieber, Science **293**, 1289 (2001).

16. A. A. Abdul-Hameed, M. Mahdi, B. Ali, A. M. Selman, H. Al-Taay, P. Jennings, and W.-J. Lee, Superlatt. Microstruc. **116**, 27 (2018).
17. D. Choi, J. Lee, M. Wober, Y.-K. Kim, H.-D. Um, and K. Seo, Device **1**, 100018 (2023).
18. A. A. Alqanoo, N. M. Ahmed, M. Hashim, M. A. Almessiere, S. A. Taya, and S. H. Zyoud, Sensors
Actuat. A: Phys. **347**, 113942 (2022).
19. S. Amdouni, Y. Cherifi, Y. Coffinier, A. Addad, M. A. Zaïbi, M. Oueslati, and R. Boukherroub, Mat. Sci. Semicond. Proces. **75**, 206 (2018).
20. U. Ray, S. Sarkar, and D. Banerjee, Catal. Today **423**, 113964 (2022).
21. S.-H. Chen, K.-Y. Kuo, K.-H. Tsai, and C.-Y. Chen, Nanomat. **12**, 1821 (2022).
22. E. Garnett and P. Yang, Nano Lett. **10**, 1082 (2010).
23. H. Al-Taay, M. Mahdi, D. Parlevliet, and P. Jennings, Mat. Sci. Semicond. Proces. **16**, 15 (2013).
24. H. Al-Taay, M. Mahdi, D. Parlevliet, Z. Hassan, and P. Jennings, Phys. E: Low-dimen. Sys. Nanostruct. **48**, 21 (2013).
25. B. P. Swain, *Advances in Nanostructured Materials*. (Singapore, Springer, 2022).
26. S. Raman, A. R. Sankar, and M. Sindhuja, Nanotech. **34** 182001 (2023).
27. Y. Lou, Z. Wang, S. Naka, and H. Okada, Phys. Proce. **14**, 204 (2011).
28. Z. Huang, N. Geyer, P. Werner, J. De Boor, and U. Gösele, Advan. Mat. **23**, 285 (2011).
29. S. Yuvaraja, V. Kumar, H. Dhasmana, A. Kumar, A. Verma, and V. Jain, J. Mat. Sci.: Mat. Electro. **30**, 7618 (2019).
30. A. A. Leonardi, M. J. L. Faro, and A. Irrera, Nanomat. **11**, 383 (2021).
31. A. Adikaari, D. Dissanayake, R. Hatton, and S. Silva, Appl. Phys. Lett. **90**, (2007).
32. T. Ameri, G. Dennler, C. Lungenschmied, and C. J. Brabec, Ener. Envir. Sci. **2**, 347 (2009).
33. S. B. Dkhil, R. Ebdelli, W. Dachraoui, H. Faltakh, R. Bourguiga, and J. Davenas, Synth. Met. **192**, 74 (2014).
34. Z. Ge, L. Xu, Y. Cao, T. Wu, H. Song, Z. Ma, J. Xu, and K. Chen, Nanosc. Res. Lett. **10**, 1 (2015).
35. S. Kato, Y. Kurokawa, K. Gotoh, and T. Soga, Appl Sci. **9**, 818 (2019).
36. N. N. Anh, N. Van Chuc, B. H. Thang, P. Van Nhat, N. Hao, D. D. Phuong, P. N. Minh, T. Subramani, N. Fukata, and P. Van Trinh, Glob. Chall. **4**, 2000010 (2020).
37. Y. Kou, K. Liu, Z. Wang, D. Chi, S. Lu, S. Yue, Y. Li, S. Qu, and Z. Wang, RSC Advan. **5**, 42341 (2015).
38. S. Thomas, N. Kalarikkal, O. S. Oluwafemi, and J. Wu, *Nanomaterials for Solar Cell Applications*. (Amsterdam, Netherlands, Elsevier, 2019).
39. A. A. Abdul-Hameed, M. Mahdi, B. Ali, A. M. Selman, H. Al-Taay, P. Jennings, and W.-J. Lee, Superlatt. Microstruct. **116**, 27 (2018).
40. V. Kumar, S. K. Sharma, T. Sharma, and V. Singh, Opt. Mat. **12**, 115 (1999).
41. Z. Bashkany, I. K. Abbas, M. Mahdi, H. Al-Taay, and P. Jennings, Silicon **10**, 403 (2018).
42. M. Naffeti, P. A. Postigo, R. Chtourou, and M. A. Zaïbi, Nanomat. **10**, 404 (2020).
43. Z. Kadhim and M. Mahdi, Phys. Scrip. **98**, 045901 (2023).
44. H. Meng, K. Fan, J. Low, and J. Yu, Dalton Trans. **45**, 13717 (2016).
45. S. Lamrani, A. Guittoum, R. Schäfer, M. Hemmous, V. Neu, S. Pofahl, T. Hadjersi, and N. Benbrahim, J. Mag. Mag. Mat. **396**, 263 (2015).
46. S. K. Srivastava, D. Kumar, S. Schmitt, K. Sood, S. Christiansen, and P. Singh, Nanotech. **25**, 175601 (2014).

47. M. Gaidi, K. Daoudi, S. Columbus, A. Hajjaji, M. A. El Khakani, and B. Bessais, J. Envir. Sci. **101**, 123 (2021).
48. Y. Jiang, R. Qing, H. Yang, C. Chen, H. Ma, and F. Chang, Appl. Phys. A **113**, 13 (2013).
49. S. Z. Khanyile, Doctor of Philosophy Thesis, University Of The Western Cape, (2021).
50. B. Qi and J. Wang, Phys. Chem. Chem. Phys. **15**, 8972 (2013).

## تصنيع وتشخيص اسلاك السليكون النانوية للخلية الشمسية غير المتجانسة

**هناء هاشم عنايه[1] و مازن عوني مهدي[1]**
*[1]قسم الفيزياء،كلية العلوم، جامعة البصرة، العراق*

الخلاصه

في هذه الدراسة، تم تحضير مصفوفات الأسلاك النانوية السليكونية بطريقة النقش الكيميائي بمساعدة المعدن (MACE) باستخدام Ag كمحفز واوقات حفر مختلفة (15، 30 و 60 دقيقة) من (100) n-Si. اذ دُرست الخواص التركيبية والموفولوجية والبصرية لاسلاك السليكون المحضرة.حيث يتراوح قطرها من 20 إلى 280 نانومتر وانعكاسها أقل من 1% في الأطوال الموجية للمنطقة المرئية لجميع العينات المحضرة. في حين كانت فجوة الطاقة أقل من 2eV تم دراسة الخصائص التركيبية باستخدام حيود الاشعة السينية حيث كانت قمم الحيود عند $2\theta = 68.7^0$ لجميع العينات المحضرة. صُنعت الخلايا الشمسية الهجينة غير المتجانسة n-SiNWs/ P3HT/PEDOT:PSS, الخلية الشمسية غير المتجانسة المصنعة لمدة 60 دقيقة لديها أكبركثافة تيار $J_{sc}$ هو $11.55\ mA.cm^{-2}$ وكفاءة تحويل 93% .0. إن الخلايا الشمسية القائمة على اسلاك السليكون غير المتجانسة المحضرة بوقت حفر 15 دقيقة لديها $J_{sc}$ و $V_{oc}$ هما $2.73\ mA/cm^2$ و 0.46 V، على التوالي ، وأقصى كفاءة تحويل 0.34%.

**الكلمات المفتاحية**: بوليمر مترافق، P3HT، SiNWs، النقش الكيميائي الكهربائي، كفاءة التحويل.